A Modified Sequence-Domain Impedance Definition and Its Equivalence to the dq-Domain Impedance Definition for the Stability Analysis of AC Power Electronic Systems

Atle Rygg, Marta Molinas, *Member, IEEE*, Chen Zhang, and Xu Cai

***Abstract*— Representation of ac power systems by frequency-dependent impedance equivalents is an emerging technique in the dynamic analysis of power systems including power electronic converters. The technique has been applied for decades in dc-power systems, and it was recently adopted to map the impedances in ac systems. Most of the work on ac systems can be categorized into two approaches. One is the analysis of the system in the *dq* domain, whereas the other applies harmonic linearization in the phase domain through symmetric components. Impedance models based on analytical calculations, numerical simulation, and experimental studies have been previously developed and verified in both domains independently. The authors of previous studies discuss the advantages and disadvantages of each domain separately, but neither a rigorous comparison nor an attempt to bridge them has been conducted. This paper attempts to close this gap by deriving the mathematical formulation that shows the equivalence between the *dq*-domain and the sequence-domain impedances. A modified form of the sequence-domain impedance matrix is proposed, and with this definition the stability estimates obtained with the generalized Nyquist criterion become equivalent in both domains. The second contribution of this paper is the definition of a *mirror frequency decoupled* (MFD) system. The analysis of MFD systems is less complex than that of non-MFD systems because the positive and negative sequences are decoupled. This paper shows that if a system is incorrectly assumed to be MFD, this will lead to an erroneous or ambiguous estimation of the equivalent impedance.**

***Index Terms*— *dq* domain, impedance, power electronic systems, sequence domain, stability analysis.**

I. Introduction

THE stability of ac power systems with a high penetration of power electronics is very difficult to analyze. The combination of multiple nonlinearities and fast dynamics stemming from controllers adds significant complexity to the analysis. Impedance-based analysis of ac power systems is a relevant and practical tool in this respect because it reduces the system into a source and load subsystem, and analyzes the dynamic interactions between the two subsystem equivalents [1], [2]. The method is based on existing techniques for dc systems, first applied in [3].

This method has some highly appealing properties. First, it considers the subsystems as black-boxes, i.e., detailed knowledge of the parameters and properties of the system is not required as long as measurements can be obtained at its terminals. Furthermore, the impedance equivalents can be extracted based on measured signals in a real system. The most accurate method for this purpose is based on frequency scanning [4]–[6]. However, this method requires advanced and dedicated equipment and has limited real-time applicability. There are several alternative methods which can estimate impedance closer to real time and with low or zero additional hardware requirements. Examples are binary sequence injection [7], impulse response [8], Kalman filtering [9], and recurrent neural networks [10]. The accuracy of these methods has not been extensively investigated in any comparative or validation studies.

When an impedance equivalent is established, it can be used for several purposes. Analytical impedance models for relatively simple systems were derived in [11]–[14]. System stability can be assessed based on these models through the generalized Nyquist criterion (GNC) [15]. Other stability criteria based on impedance models are described in [2] and [16]–[19]. Impedance equivalents have also been verified through experimental studies [11], [12], [20]–[22].

Previous work in this field can be grouped into two approaches. The first analyzes the system in the sequence domain using symmetric components (see [1], [7], [8], [23]), whereas the other applies the synchronous (*dq*) reference frame (see [2], [4], [11], [24]). Both domains have certain advantages and disadvantages, but neither a rigorous comparison nor an attempt to bridge them has yet been conducted. This paper shows mathematically how the two impedance domains are related to each other, and that they can be viewed as equivalent in terms of stability.

Manuscript received September 29, 2015; revised March 7, 2016; accepted July 5, 2016. Date of publication July 9, 2016; date of current version October 28, 2016. This work was supported in part by the Norwegian University of Science and Technology and in part by the Norwegian University of Science and Technology–Shanghai Jiao Tong University Joint Research Centre through the Norwegian Research Council. Recommended for publication by Associate Editor Dragan Maksimovic.

A. Rygg and M. Molinas are with the Department of Engineering Cybernetics, Norwegian University of Science and Technology, Trondheim 7491, Norway (e-mail: atle.rygg@ntnu.no; atlerygg@gmail.com).

C. Zhang and X. Cai are with the State Energy Smart Grid R&D Center, Shanghai Jiao Tong University, Shanghai 200240, China (e-mail: zhangchencumt@163.com; xucai@sjtu.edu.cn).

Color versions of one or more of the figures in this paper are available online at http://ieeexplore.ieee.org.

Digital Object Identifier 10.1109/JESTPE.2016.2588733

This paper makes two contributions. The first involves the proposed modified definition of the 2×2 sequence-domain impedance matrix. In this matrix, the positive and negative sequences are shifted with twice the fundamental frequency. The coupling between these two frequencies is important in power electronic systems and is defined as *the mirror frequency effect*. The equivalence between the proposed matrix and the well-established 2×2 *dq*-domain impedance matrix is derived, and it is proved that the GNC estimates are equivalent for both matrices.

The second contribution involves the definition of the *mirror frequency decoupled* (MFD) system, which is a sufficient condition to avoid the mirror frequency effect. It is shown how, in such systems, the impedance matrices become reduced. Furthermore, it is shown that the original definition of sequence-domain impedances [1] is ambiguous unless the system is MFD.

II. Relationship Between *dq* and Sequence Domains

A. Assumption: Linear Time Invariance in dq Domain

The key assumption in this paper is to consider systems that are linear time invariant (LTI) in the *dq* domain. This is a commonly applied assumption in the previous work and is often a good approximation. Some well-known contributors to violations of the assumption are the following:

1) line-commutated converters, e.g., diode rectifiers;
2) phase unbalances in impedances;
3) modulation and switching in self-commutated converters.

Even if the LTI assumption is violated, the resulting time invariance is often small. Consequently, the assumption can be applied without significant loss of accuracy.

One of the key points in this paper is to highlight that systems that are LTI in the *dq* domain might not be LTI in the phase domain. It will be shown later that a current injection at a given frequency can induce a voltage shifted by twice the fundamental frequency. This phenomenon is referred to as the *mirror frequency effect* in this paper and will occur in most systems. This definition and its applications are presented in Section IV.

B. Sequence-Domain Impedance Extraction in Previous Work

In the previous work, the sequence-domain impedances have been obtained in two ways. The most complete method takes into account phase domain unbalances [25]. The resulting impedance relation is similar to that proposed in this paper (14), but does not consider the mirror frequency effect defined in Section IV. Similarly, although (14) takes into account mirror frequency effects, it neglects phase domain unbalances.

The other, more simple method for obtaining sequence-domain impedance assumes that the positive and negative sequence are decoupled [1], [7], [12]. This is equivalent to the following definition, hereafter referred to as *original sequence-domain impedance* definition:

$$Z_p = \frac{v_p}{I_p}$$
$$Z_n = \frac{v_n}{I_n} \tag{1}$$

where Z_p is the positive sequence impedance and Z_n is the negative sequence impedance. This definition takes into account neither the sequence-domain unbalances nor the mirror frequency effect. Nonetheless, it can be accurate in many cases, in particular at high frequencies, as will be shown by simulations in Section V.

After the contributions presented in this paper were developed and submitted, another research group identified a coupling between the mirror frequencies by simulations for a case study [26]. However, no theoretical proof of the existence of such coupling was presented. In our paper, the theoretical derivations that formally prove the couplings and the equivalence between the dq and the sequence domains will be presented.

C. Harmonic Current and Voltage Equations

The first step in deriving the impedance relationship between *dq* and the sequence domains is to relate current and voltage components to each other in the two domains. This has been done in previous studies (see [27]) but the purpose of this work was not related to impedance equivalents. Reference [23] presents an impedance derivation procedure similar to the one in this paper. The derivation was here applied to a case with diagonal *dq* impedance matrix, and is hence a special case of the relations derived in the following sections.

First, the *dq* coordinate system is defined according to the Parks transform

$$\begin{bmatrix} v_d \\ v_q \end{bmatrix} = \sqrt{\frac{2}{3}} \begin{bmatrix} \cos(\theta) & \cos\left(\theta - \frac{2\pi}{3}\right) & \cos\left(\theta + \frac{2\pi}{3}\right) \\ -\sin(\theta) & -\sin\left(\theta - \frac{2\pi}{3}\right) & -\sin\left(\theta + \frac{2\pi}{3}\right) \end{bmatrix} \times \begin{bmatrix} v_a \\ v_b \\ v_c \end{bmatrix}. \tag{2}$$

For a given three-phase set of signals, v_a, v_b, v_c, the corresponding *dq*-domain signals are given by (2). θ is the transformation angle typically obtained from a phase lock loop (PLL) or from an oscillator. In steady state, $\theta = \omega_1 t$, where ω_1 is the fundamental frequency. Equation (2) is here expressed in the time domain, but is valid in the frequency domain as well. From now on, all equations are expressed in the frequency domain. The relationship between a time-domain waveform and its frequency-domain components is

$$v(t) = \sum_{k=0}^{\infty} v_k \cos(\omega_k t + \phi_k) \tag{3}$$

where v_k is the amplitude of the frequency component at frequency ω_k, and ϕ_k is the corresponding phase angle. The complex number

$$V_k = v_k e^{j\phi_k} \tag{4}$$

is defined as the harmonic phasor at frequency ω_k. From this point, the subscript k is omitted, and the relevant frequency will be indicated.

The sequence domain, also called the symmetric component domain, is widely applied in power system analysis because it can decompose unbalanced three-phase systems into three balanced and decoupled subsystems:

1) a positive sequence subsystem (p);
2) a negative sequence subsystem (n);
3) a zero sequence subsystem (0).

The effect of zero sequence components is disregarded in this paper. Note that in most applications of the sequence domain, only the fundamental frequency components are considered, whereas in this paper the phasors can be related to any frequency. *abc* phasors can be related to sequence-domain phasors by the symmetric component transform

$$\begin{bmatrix} V_p \\ V_n \end{bmatrix} = \begin{bmatrix} 1 & a & a^2 \\ 1 & a^2 & a \end{bmatrix} \begin{bmatrix} V_a \\ V_b \\ V_c \end{bmatrix} \tag{5}$$

where V_p is the *positive sequence* voltage phasor, and V_n is the *negative sequence* voltage phasor at an arbitrary frequency. $a = e^{j(2\pi/3)}$ is the complex number corresponding to a 120° phase shift. It can be shown that sequence-domain phasors are related to *dq*-domain phasors as follows:

$$\begin{bmatrix} V_p \\ V_n \end{bmatrix} = \frac{1}{\sqrt{6}} \begin{bmatrix} V_d + jV_q \\ 0 \end{bmatrix}, \quad \omega_p = \omega_{dq} + \omega_1$$
$$\begin{bmatrix} V_p \\ V_n \end{bmatrix} = \frac{1}{\sqrt{6}} \begin{bmatrix} 0 \\ V_d - jV_q \end{bmatrix}, \quad \omega_n = \omega_{dq} - \omega_1. \tag{6}$$

In other words, a general *dq* voltage phasor at a frequency ω_{dq} is equivalent to two sequence-domain voltage phasors at different frequencies, shifted by the fundamental:

1) positive sequence voltage at $\omega_p = \omega_{dq} + \omega_1$;
2) negative sequence voltage at $\omega_n = \omega_{dq} - \omega_1$.

Similarly, it can be shown that for a given positive or negative sequence voltage phasor, the corresponding *dq*-domain phasors are

$$\begin{bmatrix} V_d \\ V_q \end{bmatrix} = \sqrt{\frac{3}{2}} V_p \begin{bmatrix} 1 \\ -j \end{bmatrix}, \quad \omega_{dq} = \omega_p - \omega_1$$
$$\begin{bmatrix} V_d \\ V_q \end{bmatrix} = \sqrt{\frac{3}{2}} V_n \begin{bmatrix} 1 \\ j \end{bmatrix}, \quad \omega_{dq} = \omega_n + \omega_1. \tag{7}$$

By definition, (2)–(7) also apply to currents.

D. Illustration of Harmonic Phasor Relations

Equation (6) is illustrated in Fig. 1. A perturbation in a *dq*-domain current waveform at a randomly selected frequency of 80 Hz is modeled as follows:

$$\left.\begin{aligned} I_d &= 2\angle 80^\circ \\ I_q &= 3\angle 30^\circ \end{aligned}\right\}, \quad \omega_{dq} = 2\pi \cdot 80. \tag{8}$$

The waveform is expressed in the *abc* domain using the inverse of (2). Fast Fourier transform is used to calculate the frequency domain harmonic phasors in both domains. These are drawn in the complex plane in Fig. 1. It is seen that the single *dq* tone at 80 Hz is transformed into 30- and 130-Hz components in the *abc* domain. Moreover, it is seen that the 30-Hz waveforms are pure negative sequences, whereas the 130-Hz waveforms are pure positive sequences, which is consistent with (6). The sequence-domain phasors are calculated from the *dq*-domain phasors by this equation. Note also that the sequence-domain phasors satisfy the following equation for balanced *abc* components: $I_{ap} = I_p$ and $I_{an} = I_n$.

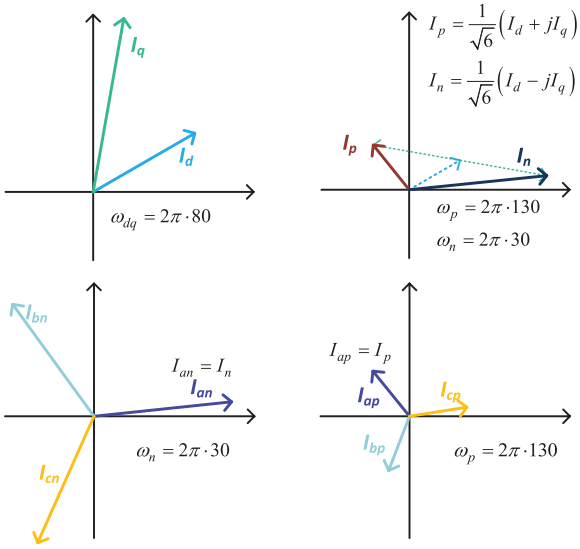

Fig. 1. Harmonic phasors corresponding to (8). The 80-Hz waveform at ω_{dq} equals the sum of a positive sequence waveform at $\omega_p = \omega_{dq} + \omega_1$ and a negative sequence waveform at $\omega_n = \omega_{dq} - \omega_1$.

TABLE I
OVERVIEW OF CURRENTS, VOLTAGES, AND IMPEDANCES AND THE CORRESPONDING FREQUENCIES AT WHICH THEY ARE DEFINED

Parameter	Frequency
V_d , I_d	ω_{dq}
V_q , I_q	ω_{dq}
$\boldsymbol{Z_{dq}}$	ω_{dq}
V_p , I_p	$\omega_p = \omega_{dq} + \omega_1$
V_n , I_n	$\omega_n = \omega_{dq} - \omega_1$
Z_{pp}	ω_p
Z_{nn}	ω_n
Z_{pn}	$\omega_n \rightarrow \omega_p$
Z_{np}	$\omega_p \rightarrow \omega_n$
Z_p	ω_p
Z_n	ω_n

III. MODIFIED SEQUENCE-DOMAIN IMPEDANCE DEFINITION

In the previous section, current and voltage phasors were considered separately. This section will relate them to each other through impedance. The main contribution of this paper is then outlined, which is a 2×2 impedance matrix composed of positive and negative sequence impedances at two different frequencies. The proposed 2×2 matrix has many appealing properties, as will be highlighted in further sections.

To provide a better overview, all currents, voltages, and impedances are summarized in Table I. These definitions highlight a key point in this paper: positive and negative sequences are defined at two different frequencies, shifted by twice the fundamental frequency. The two frequencies are also called *mirror frequencies* later in this paper.

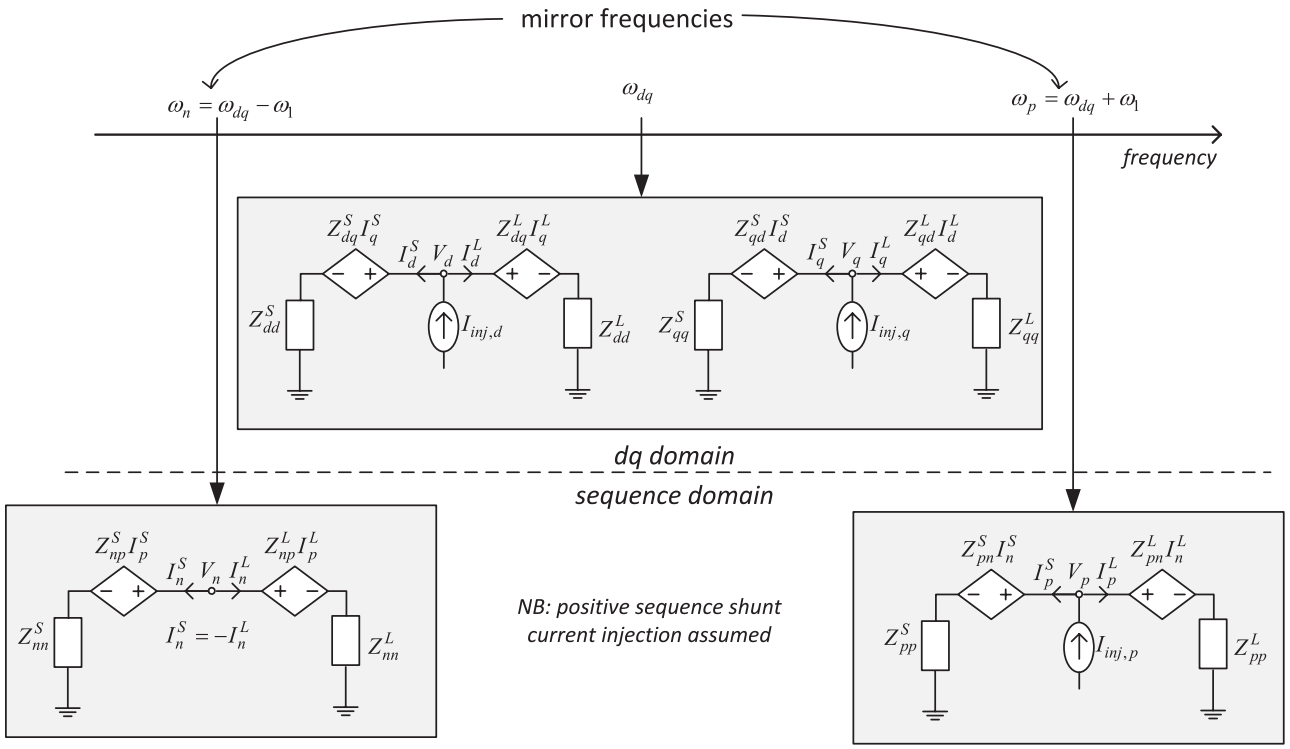

Fig. 2. Circuit equivalents of impedance equations in the *dq* and sequence domains. Mirror frequency coupling illustrated by voltage sources in the sequence domain.

A. Definition and Fundamental Equations

The basis for the following derivations is the generalized Ohm's law in the *dq* domain:

$$\begin{bmatrix} V_d \\ V_q \end{bmatrix} = \begin{bmatrix} Z_{dd} & Z_{dq} \\ Z_{qd} & Z_{qq} \end{bmatrix} \begin{bmatrix} I_d \\ I_q \end{bmatrix} = \boldsymbol{Z_{dq}} \begin{bmatrix} I_d \\ I_q \end{bmatrix} \tag{9}$$

where $\boldsymbol{Z_{dq}}$ is a 2×2 matrix of complex numbers as a function of frequency. This equation will now be transformed into the sequence domain.

As shown by (7), any set of *dq*-domain phasors can be written as the sum of positive sequence phasors at $\omega_{dq}+\omega_1$ and negative sequence phasors at $\omega_{dq} - \omega_1$. Substituting from (7) gives a modified version of (9)

$$V_p \begin{bmatrix} 1 \\ -j \end{bmatrix} + V_n \begin{bmatrix} 1 \\ j \end{bmatrix} = \boldsymbol{Z_{dq}} \left(I_p \begin{bmatrix} 1 \\ -j \end{bmatrix} + I_n \begin{bmatrix} 1 \\ j \end{bmatrix} \right). \tag{10}$$

The definitions shown in Table I are based on this convenient representation. The next step is to multiply (10) with (1/2)[1 j] and (1/2)[1 $-j$], leading to the following two equations:

$$\begin{aligned} V_p &= I_p \left(\frac{1}{2} [1 \quad j] \boldsymbol{Z_{dq}} \begin{bmatrix} 1 \\ -j \end{bmatrix} \right) + I_n \left(\frac{1}{2} [1 \quad j] \boldsymbol{Z_{dq}} \begin{bmatrix} 1 \\ j \end{bmatrix} \right) \\ V_n &= I_p \left(\frac{1}{2} [1 \quad -j] \boldsymbol{Z_{dq}} \begin{bmatrix} 1 \\ -j \end{bmatrix} \right) + I_n \left(\frac{1}{2} [1 \quad -j] \boldsymbol{Z_{dq}} \begin{bmatrix} 1 \\ j \end{bmatrix} \right). \end{aligned} \tag{11}$$

Equation (11) can conveniently be rewritten with matrix notation by defining the *modified sequence-domain impedance matrix*

$$\begin{bmatrix} V_p \\ V_n \end{bmatrix} = \begin{bmatrix} Z_{pp} & Z_{pn} \\ Z_{np} & Z_{nn} \end{bmatrix} \begin{bmatrix} I_p \\ I_n \end{bmatrix} = \boldsymbol{Z_{pn}} \begin{bmatrix} I_p \\ I_n \end{bmatrix} \tag{12}$$

with the four impedances substituted from (11)

$$\boldsymbol{Z_{pn}} = \frac{1}{2} \begin{bmatrix} [1 \quad j] \boldsymbol{Z_{dq}} \begin{bmatrix} 1 \\ -j \end{bmatrix} & [1 \quad j] \boldsymbol{Z_{dq}} \begin{bmatrix} 1 \\ j \end{bmatrix} \\ [1 \quad -j] \boldsymbol{Z_{dq}} \begin{bmatrix} 1 \\ -j \end{bmatrix} & [1 \quad -j] \boldsymbol{Z_{dq}} \begin{bmatrix} 1 \\ j \end{bmatrix} \end{bmatrix}. \tag{13}$$

The impedances have the following physical interpretation.

1) Z_{pp}*:* measures the positive sequence voltage at ω_p induced by a positive sequence current at ω_p.
2) Z_{pn}*:* measures the positive sequence voltage at ω_p induced by negative sequence current at ω_n.
3) Z_{np}*:* measures the negative sequence voltage at ω_n induced by positive sequence current at ω_p.
4) Z_{nn}*:* measures the negative sequence voltage at ω_n induced by a negative sequence current at ω_n.

Equation (13) can be rewritten in a more compact form as a linear transformation by the unitary matrix A_Z

$$\begin{aligned} \boldsymbol{Z_{pn}} &= A_Z \cdot \boldsymbol{Z_{dq}} \cdot A_Z^{-1} \\ \boldsymbol{Z_{dq}} &= A_Z^{-1} \cdot \boldsymbol{Z_{pn}} \cdot A_Z \\ A_Z &= \frac{1}{\sqrt{2}} \begin{bmatrix} 1 & j \\ 1 & -j \end{bmatrix}, \quad A_Z^{-1} = A_Z^* = \frac{1}{\sqrt{2}} \begin{bmatrix} 1 & 1 \\ -j & j \end{bmatrix} \end{aligned} \tag{14}$$

where * denotes complex conjugate transpose.

The corresponding admittance equations can be obtained in the same way by interchanging voltages with currents in the derivation process

$$\begin{aligned} \boldsymbol{Y_{pn}} &= A_Z \cdot \boldsymbol{Y_{dq}} \cdot A_Z^{-1} \\ \boldsymbol{Y_{dq}} &= A_Z^{-1} \cdot \boldsymbol{Y_{pn}} \cdot A_Z. \end{aligned} \tag{15}$$

The generalized Ohm's law and the mirror frequency effect are illustrated as circuit equivalents in Fig. 2.

TABLE II
EXAMPLE OF *dq*- AND SEQUENCE-DOMAIN FREQUENCIES

ω_{dq}	ω_p	ω_n
500	550	450
120	170	70
65	115	15
40	90	-10→10*
15	65	-35→35*

* negative sequence frequencies where the impedances are transformed to positive sequence as explained in section III-B

The figure assumes positive sequence shunt current injection at frequency ω_p, but corresponding equivalents can be made for other injection choices. In the *dq* domain, all signals are expressed using the same frequency ω_{dq}. The cross-coupling between the *d*- and *q*-axis is represented by current-dependent voltage sources.

B. Positive Sequence Impedances Below the Fundamental Frequency

In this paper, the modified sequence-domain impedance has thus far not been defined for positive sequence at frequencies below the fundamental frequency. Given that $\omega_p = \omega_{dq} + \omega_1$, the *dq*-domain frequency ω_{dq} will be negative for $0 \leq \omega_p < \omega_1$. To extend the impedance definition to positive sequence below the fundamental frequency, it is first important to note that a balanced three-phase signal with a negative frequency is equivalent to a balanced three-phase signal with positive frequency at the same absolute value. Only the phase order needs to be changed, i.e., a positive sequence signal becomes a negative sequence, and vice versa.

Second, note that when $0 \leq \omega_{dq} < \omega_1$, the negative sequence frequency $\omega_n = \omega_{dq} - \omega_1$ is negative. Consequently, the negative sequence impedance Z_{nn} is associated with a negative frequency. Based on the discussion above, the negative sequence impedance at a negative frequency is equal to the positive sequence impedance at a positive frequency with the same absolute value. Thus, a positive sequence impedance below the fundamental frequency can be defined.

To summarize, an example of *dq* domain and the corresponding sequence-domain frequencies are given in Table II.

C. Nyquist Stability Criterion Equivalence

The GNC has been widely applied in previous studies to analyze the stability of power electronics systems (see [13], [18], [21]). The criterion is mathematically formulated in [15], and was first applied to ac power electronic systems in [2]. It will now be shown that when the GNC is applied to the *dq* and the modified sequence domains, the results are identical.

Assuming the *dq* domain, the basis for the stability criterion is the system transfer function between the source and the load

$$\boldsymbol{h} = \mathrm{inv}\big(\boldsymbol{I} + \boldsymbol{Z}_{\boldsymbol{dq}}^{\boldsymbol{S}}\boldsymbol{Y}_{\boldsymbol{dq}}^{\boldsymbol{L}}\big). \tag{16}$$

For convenience, the minor-loop gain $\boldsymbol{L_{dq}}$ is defined as

$$\boldsymbol{L_{dq}} = \boldsymbol{Z}_{\boldsymbol{dq}}^{\boldsymbol{S}}\boldsymbol{Y}_{\boldsymbol{dq}}^{\boldsymbol{L}}. \tag{17}$$

The eigenvalues of $\boldsymbol{L_{dq}}$ can be found by solving

$$\det(\boldsymbol{L_{dq}} + \lambda_{dq}\boldsymbol{I}) = 0. \tag{18}$$

Assume in the following that the source is stable when connected to an ideal load, and that the load is stable when connected to an ideal source. The GNC then states that the system is stable if and only if the characteristic loci of $\boldsymbol{L_{dq}}$ do not encircle the point $(-1, 0)$ when drawn in the complex plane.

The minor-loop gain in the sequence domain can be expressed as

$$\begin{aligned}\boldsymbol{L_{pn}} &= \boldsymbol{Z}_{\boldsymbol{pn}}^{\boldsymbol{S}}\boldsymbol{Y}_{\boldsymbol{pn}}^{\boldsymbol{L}} = \big(A_Z \cdot \boldsymbol{Z}_{\boldsymbol{dq}}^{\boldsymbol{S}} \cdot A_Z^{-1}\big)\big(A_Z \cdot \boldsymbol{Y}_{\boldsymbol{dq}}^{\boldsymbol{L}} \cdot A_Z^{-1}\big) \\ &= A_Z \cdot \boldsymbol{Z}_{\boldsymbol{dq}}^{\boldsymbol{S}}\boldsymbol{Y}_{\boldsymbol{dq}}^{\boldsymbol{L}} \cdot A_Z^{-1} = A_Z \cdot \boldsymbol{L_{dq}} \cdot A_Z^{-1}.\end{aligned} \tag{19}$$

The following equations prove that λ_{dq}, the eigenvalues of $\boldsymbol{L_{dq}}$, are equal to λ_{pn}, the eigenvalues of $\boldsymbol{L_{pn}}$:

$$\begin{aligned}0 &= \det(\boldsymbol{L_{pn}} - \lambda_{pn}\boldsymbol{I}) = \det\big(A_Z \cdot \boldsymbol{L_{dq}} \cdot A_Z^{-1} - \lambda_{pn}\boldsymbol{I}\big) \\ &= \det\big(A_Z \cdot \boldsymbol{L_{dq}} \cdot A_Z^{-1} - A_Z \cdot (\lambda_{pn}\boldsymbol{I}) \cdot A_Z^{-1}\big) \\ &= \det(A_Z) \cdot \det(\boldsymbol{L_{dq}} - \lambda_{pn}\boldsymbol{I}) \cdot \det\big(A_Z^{-1}\big) \\ &= \det(\boldsymbol{L_{dq}} - \lambda_{pn}\boldsymbol{I}) = 0 \\ &\Rightarrow \lambda_{pn} = \lambda_{dq}.\end{aligned} \tag{20}$$

Consequently, the stability analysis by GNC gives identical results in the *dq* and sequence domains when the *modified* definition (14) is applied. By contrast, if the *original* definition (1) is used, and one or both subsystems are *not* MFD (see Section IV), the calculated stability is different from the *dq*-domain stability calculations.

IV. MIRROR FREQUENCY EFFECT

The term *mirror frequency effect* is defined in this paper to provide further insight into the properties of impedance models. It has been shown that systems that are LTI in the *dq* domain may not be LTI in the phase domain by the original impedance definitions. However, it has also been shown that the modified sequence domain is defined in such a way that any LTI system in the *dq* domain is also LTI in the modified sequence domain.

This section explores the conditions for systems to be LTI under the original sequence domain definition. This is related to the mirror frequency effects, and such systems will hereafter be referred to as *MFD*.

A. Mirror Frequency Decoupled Systems

A subsystem is said to be MFD if, when subjected to a harmonic disturbance at an arbitrary frequency, it only responds with current/voltages at the same frequency. In other words, it is LTI in the original sequence domain. With reference to Fig. 2, this is equivalent to removing the current-dependent voltage sources in the sequence domain, i.e., $Z_{pn} = Z_{np} = 0$. MFD systems have several interesting properties presented as follows.

B. Impedance Matrices of MFD Systems

MFD subsystems have sequence- and dq-domain impedance matrices of the following form:

$$\boldsymbol{Z_{pn}}|_{\text{MFD}} = \begin{bmatrix} Z_{pp} & 0 \\ 0 & Z_{nn} \end{bmatrix}$$
$$\boldsymbol{Z_{dq}}|_{\text{MFD}} = \begin{bmatrix} Z_{\text{diag}} & Z_{\text{offdiag}} \\ -Z_{\text{offdiag}} & Z_{\text{diag}} \end{bmatrix} \tag{21}$$

where $Z_{pn} = Z_{np} = 0$ by MFD definition. The dq-domain matrix in an MFD system has $Z_{dd} = Z_{qq} = Z_{\text{diag}}$ and $Z_{dq} = -Z_{qd} = Z_{\text{offdiag}}$. The proof of these relations is presented in Appendix C. In [23], a similar result was found under the assumption of $Z_{dq} = Z_{qd} = 0$. Since $\mathbf{Z_{pn}}$ is diagonal, the original impedance definition (1) is equivalent to the modified (14) for MFD systems.

C. dq Impedance Extraction in MFD Systems

It has been argued that sequence-domain impedances are easier to obtain than dq-domain impedances due to the decoupling between positive and negative sequences [1], [12]. Furthermore, the sequence-domain impedance can be obtained from a single measurement with no need for matrix inversions because of this decoupling. However, it has been shown in the previous section that sequence-domain impedances can been assumed to be decoupled only if the subsystem is MFD. In contrast with the statements of previous work, the following equations show that dq-domain impedances can also be obtained from a single measurement in this case. Combining (9) with (21) gives

$$Z_{\text{diag}} = Z_{dd} = Z_{qq} = \frac{V_d I_d + V_q I_q}{I_d^2 + I_q^2}$$
$$Z_{\text{offdiag}} = Z_{dq} = -Z_{qd} = \frac{V_d I_q - V_q I_d}{I_d^2 + I_q^2}. \tag{22}$$

Consequently, only a single measurement is needed to obtain the dq impedance matrix in an MFD subsystem.

D. Sources to Mirror Frequency Coupling

Mirror frequency coupling is introduced in all parts of the power system where (21) is not satisfied. They include the following:

1) PLL;
2) converter current controllers with unequal structure and/or parameter values in the d- and q-axis;
3) dc-link voltage control systems;
4) active and reactive power controllers;
5) salient-pole synchronous machines.

The analytical impedance calculation in the dq domain is described in [11], where the coupling related to the first four items mentioned above can be identified. Note that all transfer functions must be identical in d- and q-axis in order for the subsystem to be MFD. Furthermore, all cross-coupling between d- and q-axis must have opposite sign. The synchronous machine is also mentioned because it is a vital part of many power systems, and it possesses mirror frequency coupling if the reluctance in d- and q-axes differ.

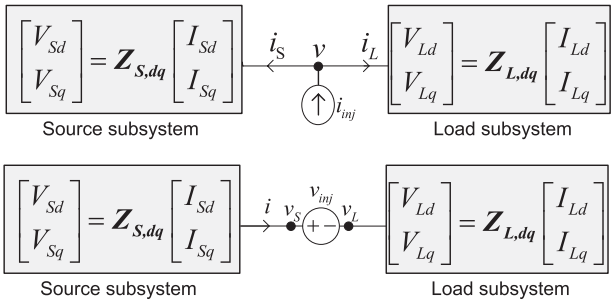

Fig. 3. Illustration of the two injection methods (shunt and series) for a general source and load subsystem.

Although mirror frequency coupling is independent of power electronics, it is clear from the points above that power electronics systems introduce many instances for this to occur.

V. Validation by Numeric Simulation

A. Obtaining Impedances Through Simulation

The method for obtaining impedances through simulation is best explained by the circuit diagrams in Fig. 3 and the flowchart in Fig. 4. This method is able to calculate both the dq-domain and sequence-domain impedances in an integrated process. The first step is to select a vector of frequencies $f_{dq,\text{tab}}$, i.e., the frequencies at which the impedances shall be calculated. Note that these frequencies are expressed in the dq domain.

The system can be simulated under either shunt current or series voltage injection. The difference between these two methods is illustrated in Fig. 3. If shunt current is used, the following three-phase perturbation signals will be injected:

$$i_{inj1} = I_{inj} \begin{bmatrix} \sin([\omega_{inj} + \omega_1]t) \\ \sin\left([\omega_{inj} + \omega_1]t - \frac{2\pi}{3}\right) \\ \sin\left([\omega_{inj} + \omega_1]t + \frac{2\pi}{3}\right) \end{bmatrix}$$
$$i_{inj2} = I_{inj} \begin{bmatrix} \sin([\omega_{inj} - \omega_1]t) \\ \sin\left([\omega_{inj} - \omega_1]t + \frac{2\pi}{3}\right) \\ \sin\left([\omega_{inj} - \omega_1]t - \frac{2\pi}{3}\right) \end{bmatrix}. \tag{23}$$

If series voltage injection is applied, i can be replaced with v. The two sets of signals need to have different frequencies because linearly independent injections are required when solving for the impedance matrices (24) and (25). The selection of injection signals is discussed in [4].

The needed outputs from simulations are the current and voltage signals shown in Fig. 3. Note that the injection signal itself is not needed in impedance calculations. After converting time-domain signals to the frequency domain as described in the flowchart, the following equations can be used to find the impedances in the two domains:

$$\begin{bmatrix} Z_{dd} & Z_{dq} \\ Z_{qd} & Z_{qq} \end{bmatrix} = \begin{bmatrix} V_{d1} & V_{d2} \\ V_{q1} & V_{q2} \end{bmatrix} \begin{bmatrix} I_{d1} & I_{d2} \\ I_{q1} & I_{q2} \end{bmatrix}^{-1} \tag{24}$$
$$\begin{bmatrix} Z_{pp} & Z_{pn} \\ Z_{np} & Z_{nn} \end{bmatrix} = \begin{bmatrix} V_{p1} & V_{p2} \\ V_{n1} & V_{n2} \end{bmatrix} \begin{bmatrix} I_{p1} & I_{p2} \\ I_{n1} & I_{n2} \end{bmatrix}^{-1}. \tag{25}$$

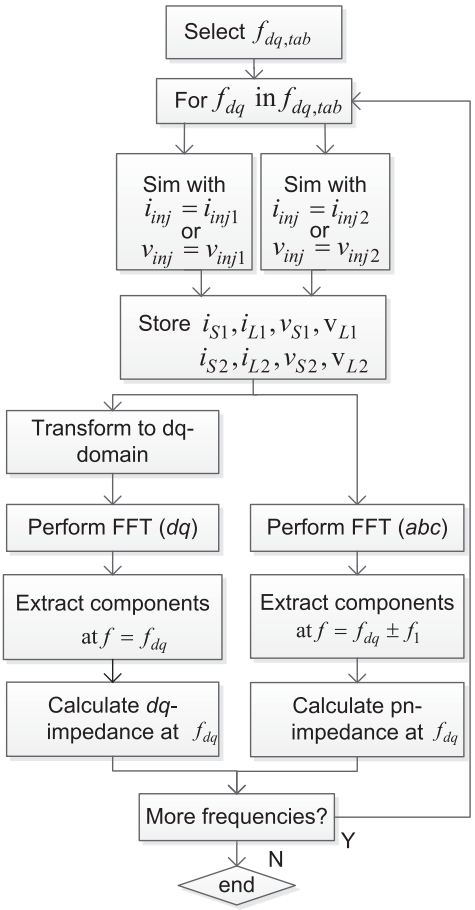

Fig. 4. Illustration of simulation method to obtain both *dq*- and sequence-domain impedances as a function of frequency. The flowchart is valid for both shunt current and series voltage injection.

After these two matrices are established, all other impedance expressions in the paper can be derived based on them.

B. Case Study Description

In this section, the validity of the previously derived expressions is checked through numeric simulations. Simulation cases A and B are developed in MATLAB/Simulink (see Figs. 5 and 6). Both cases consist of a source converter and a load converter. The control systems operate in the *dq* domain.

In case A, the source converter controls the voltage v according to set points and the virtual inductances L_{vd} and L_{vq}. The converter is synchronized to the fixed clock signal $\theta_S = 2\pi f_n \cdot t$. The load converter operates with dc-voltage control and reactive current control, and a current source I_{dc} consumes power at the dc side. The converter is synchronized to the grid by a PLL.

The following sources to mirror frequency coupling are present in case A *source subsystem*:

1) $L_{vd} \neq L_{vq}$;
2) $K_{pvd} \neq K_{pvq}$;
3) $T_{ivd} \neq T_{ivq}$.

In case A *load subsystem*, the following sources to mirror frequency coupling are present:

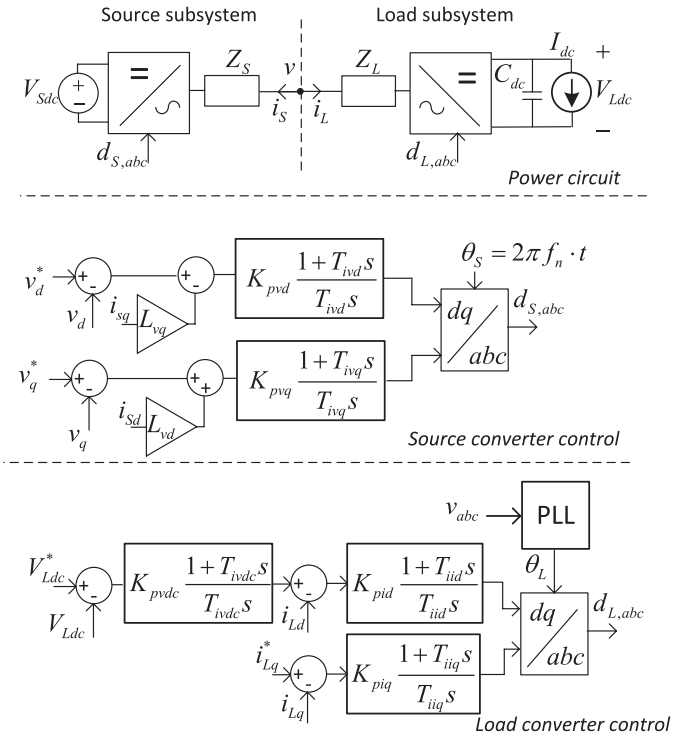

Fig. 5. Detailed schematic of case A.

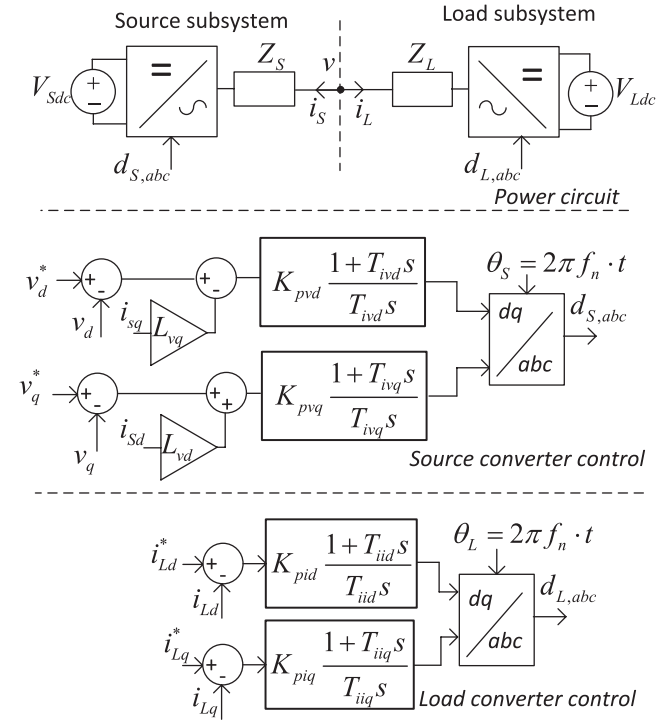

Fig. 6. Detailed schematic of case B.

1) DC-link voltage controller;
2) PLL is connected to a non-stiff point in the grid;
3) $K_{pid} \neq K_{piq}$;
4) $T_{pid} \neq T_{piq}$.

To better illustrate the findings in the paper, case A has been divided into two subcases, case A1 and case A2. In case A1, both subsystems are mirror frequency coupled according to

the lists above. However, in case A2, all mirror frequency couplings in the source subsystem are removed by setting $L_{vd} = L_{vq}$, $K_{pvd} = K_{pvq}$ and $T_{ivd} = T_{ivq}$. Hence, in case A2, the source subsystem is MFD, while the load subsystem is not. The differences between these two cases will be discussed in the section V.C.

In case B, all mirror frequency couplings are removed in both subsystems, leading to a complete MFD system. The source subsystem is identical to the one in case A2. In the load subsystem, the converter is connected to a constant voltage at the dc side, which eliminates the need for dc voltage control. The control system consists of current controllers with set points i^*_{Ld} and i^*_{Ld}. The Proportional Integral (PI)-controller parameters are identical in d- and q-axis. Furthermore, the converter does not contain a PLL, but is instead synchronized to the fixed ramp $\theta_L = 2\pi f_n \cdot t$ in the same way as the source converter. Consequently, all mirror frequency coupling sources from the above list have been removed.

Parameter values applied in the simulation cases are given in Appendix A.

C. Simulation Results—$\boldsymbol{Z_{dq}}$ and $\boldsymbol{Z_{pn}}$

The resulting impedance curves for the three cases are shown in Figs. 7–9 for the dq domain and in Figs. 10–12 for the modified sequence domain. Only magnitude is presented in these figures for simplicity, but it has been verified that the angles are consistent with the conclusions. Impedances for the load and source subsystems are plotted in the same graph. In the sequence-domain plots, impedances have been obtained in two ways, denoted by subscript a and b:

1) Z_a: direct simulation of $\boldsymbol{Z_{pn}}$ using (25);
2) Z_b: based on simulated $\boldsymbol{Z_{dq}}$ from (24) and the transform given by $\boldsymbol{Z_{pn}} = A_Z \cdot \boldsymbol{Z_{dq}} \cdot A_Z^{-1}$ (14).

The following observations support the claims in the previous sections.

1) The two ways of obtaining modified sequence-domain impedances (Z_a and Z_b) produce identical results in all cases. This confirms the transformation relationship from dq to sequence domain (14).
2) In case A1, there are no symmetries in the impedance curves, neither in dq nor in sequence domain. This is expected since both subsystems have mirror frequency coupling.
3) In case A2, $Z^S_{pn} \approx Z^S_{np} \approx 0$, as expected since the source subsystem is MFD [see also (21)].
4) In case B, $Z_{pn} \approx Z_{np} \approx 0$ for both subsystems. This is expected since both subsystems are MFD. It can also be observed that $Z_{dq} = -Z_{qd}$ and $Z_{dd} = Z_{qq}$ for both subsystems, again according to (21).

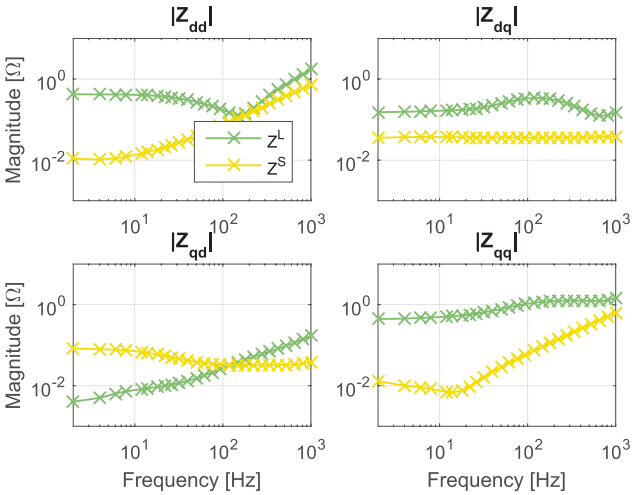

Fig. 7. Case A1 dq-domain impedances for both subsystems.

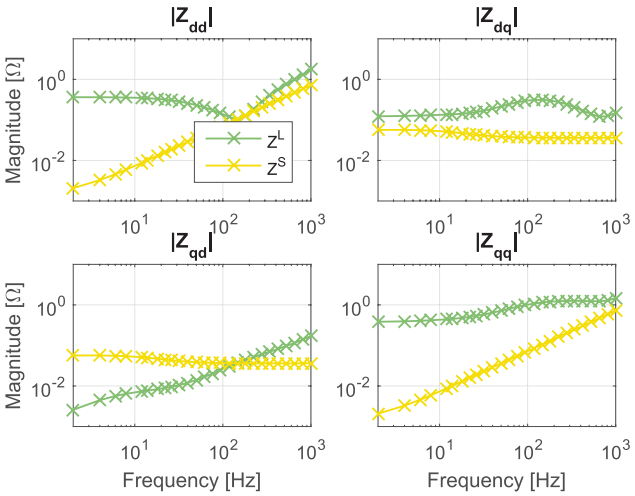

Fig. 8. Case A2 dq-domain impedances for both subsystems.

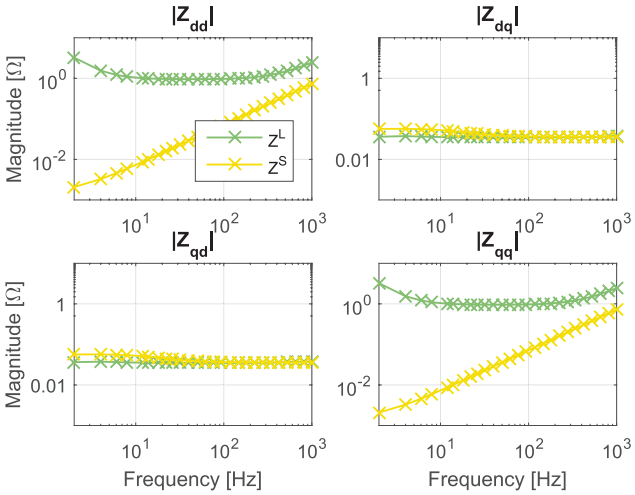

Fig. 9. Case B dq-domain impedances for both subsystems.

D. Simulation Results—Modified Versus Original

The purpose of this section is to investigate the validity of the equations derived in Appendix D and to determine how the original and modified sequence-domain impedances relate to each other. Figs. 13–15 present the same comparison for each of the three simulation cases. Only the *load subsystem* impedance is included in the comparison. The original sequence-domain impedances, Z_p and Z_n, are compared with the diagonal elements in the modified sequence-domain impedance matrix, Z_{pp} and Z_{nn}. Furthermore, the original

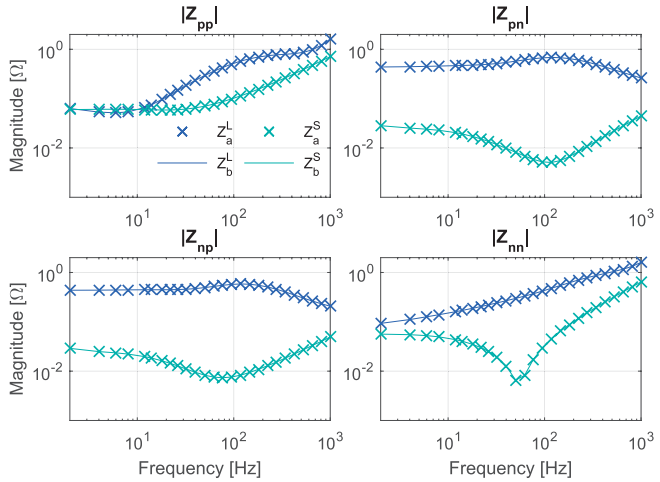

Fig. 10. Case A1 sequence-domain impedances for both subsystems. *a* and *b* indicate two calculation methods.

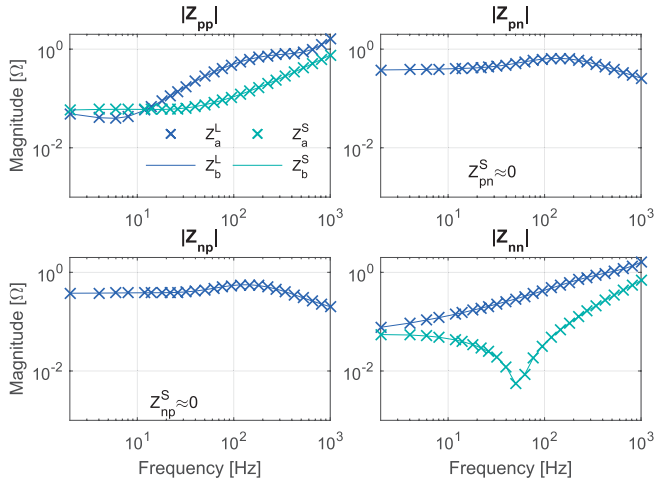

Fig. 11. Case A2 sequence-domain impedances for both subsystems. *a* and *b* indicate two calculation methods.

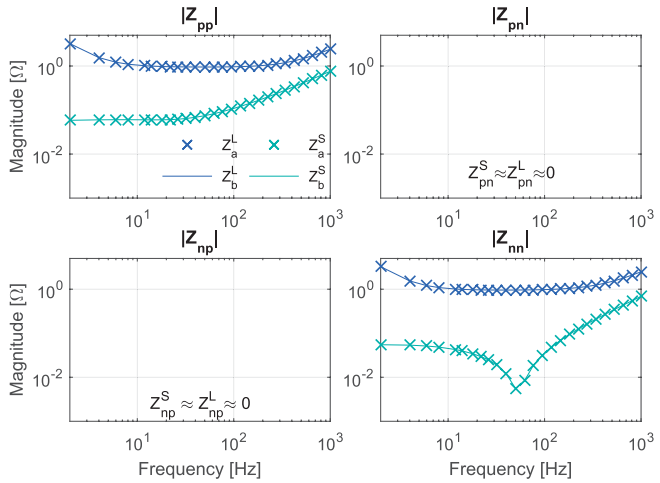

Fig. 12. Case B sequence-domain impedances for both subsystems. *a* and *b* indicate two calculation methods.

sequence-domain impedances are simulated both by shunt current and series voltage injection. Additionally, they are estimated in two ways to validate the equations derived in Appendix D. Table III summarizes the notation and estimation methods.

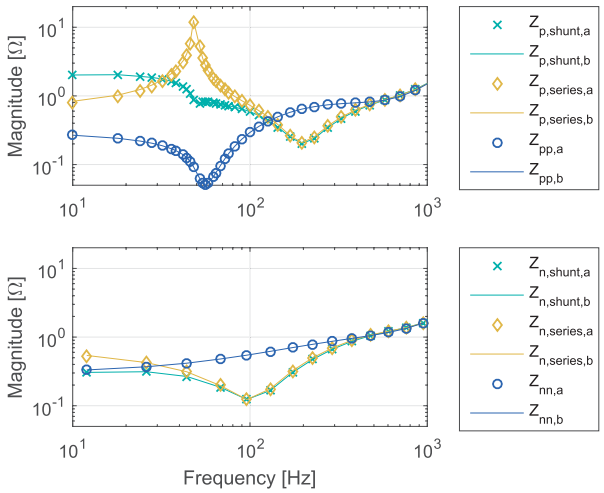

Fig. 13. Comparison of *load subsystem* original and modified sequence-domain impedances in case A1.

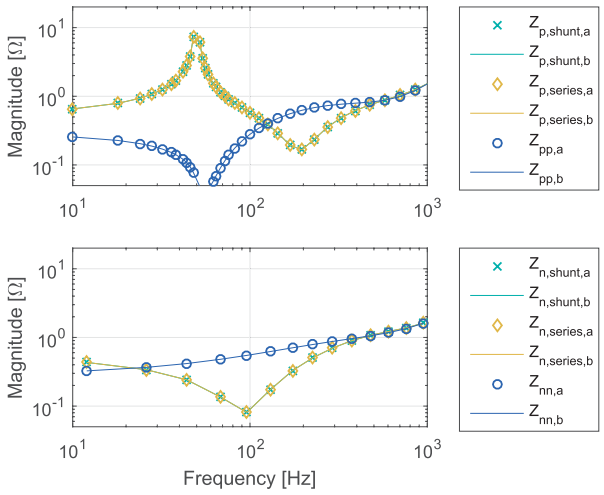

Fig. 14. Comparison of *load subsystem* original and modified sequence-domain impedances in case A2.

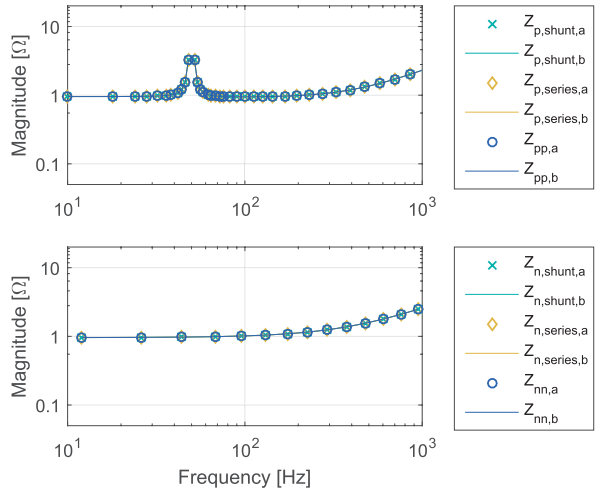

Fig. 15. Comparison of *load subsystem* original and modified sequence-domain impedances in case B.

First, it can be noted that the methods based on direct simulations always overlap with the calculated one for all three cases, which validates (14), (30), and (33).

TABLE III
EXPLANATION OF THE LEGENDS IN FIGS. 13–15

Legend notation	Eq. notation	Estimation mehtod
$Z_{p,shunt,a}$	$Z_p^L\|_{shunt}$	Direct simulation using (1)
$Z_{p,shunt,b}$	$Z_p^L\|_{shunt}$	Calculation based on simulated $\boldsymbol{Z_{pn}}$ from (25) and the formula (30)
$Z_{p,series,a}$	$Z_p^L\|_{series}$	Direct simulation using (1)
$Z_{p,series,b}$	$Z_p^L\|_{series}$	Calculation based on simulated $\boldsymbol{Z_{pn}}$ from (25) and the formula (33)
$Z_{pp,a}$	Z_{pp}^L	Direct simulation using (25)
$Z_{pp,b}$	Z_{pp}^L	Calculation based simulated $\boldsymbol{Z_{dq}}$ from (24) and the formula (14)

In case A1, the original impedances obtained by shunt and series injection are not equal. This is expected based on the difference between (30) and (33). The difference is noticeable at frequencies below 100 Hz. It is also observed that the modified sequence impedances Z_{pp} and Z_{nn} deviate substantially from the original ones at frequencies up to $\approx$ 500 Hz; however, after this point they are close to equal. Consequently, the load subsystem can be assumed to be MFD for frequencies above 500 Hz.

In case A2, it is clear that the load subsystem impedances obtained from shunt and series injection are equal. This is consistent with (35), because the source subsystem is MFD in this case. The same equation gives $Z_{pp} \neq Z_p$ and $Z_{nn} \neq Z_n$, which is verified by the figure. However, the difference is close to zero at frequencies above $\approx$ 500 Hz, similar to case A1.

In case B, all impedance estimates coincide. From (36) we have that $Z_p = Z_{pp}$ and $Z_n = Z_{nn}$ whenever $Z_{pn} = Z_{np} = 0$. Both systems are now MFD, and hence the assumption of decoupled sequence domain is valid.

E. Simulation Results—Generalized Nyquist Criterion

It has been shown in Section III-C that the GNC will give the same result in the *dq* domain and the modified sequence domain. Furthermore, it has been shown that the stability analysis based on original sequence-domain impedances will give different results unless both subsystems are MFD. This has been investigated by applying the GNC to the impedance curves found in Figs. 7–15. The resulting Nyquist plots are presented in Fig. 16. Note that only the most critical eigenvalue is plotted, corresponding to the operating point of $i_{sd} = 1.1$ pu.

In all cases, the *dq* domain gives exactly the same result as the modified sequence domain. On the other hand, the original sequence-domain impedances do not give the same Nyquist plot in cases A1 and A2. In case B, all methods give the same Nyquist curves.

F. Time-Domain Analysis

To complement the stability analysis from the previous section, a time-domain simulation has been conducted and presented in Fig. 17. Cases A1 and A2 are used for the simulation (see Fig. 5 for the system block diagram). The power consumed by the load converter is stepwise increased by applying step changes to I_{dc}. Fig. 17 shows the resulting *dq* currents at the *source converter*. The transient oscillations

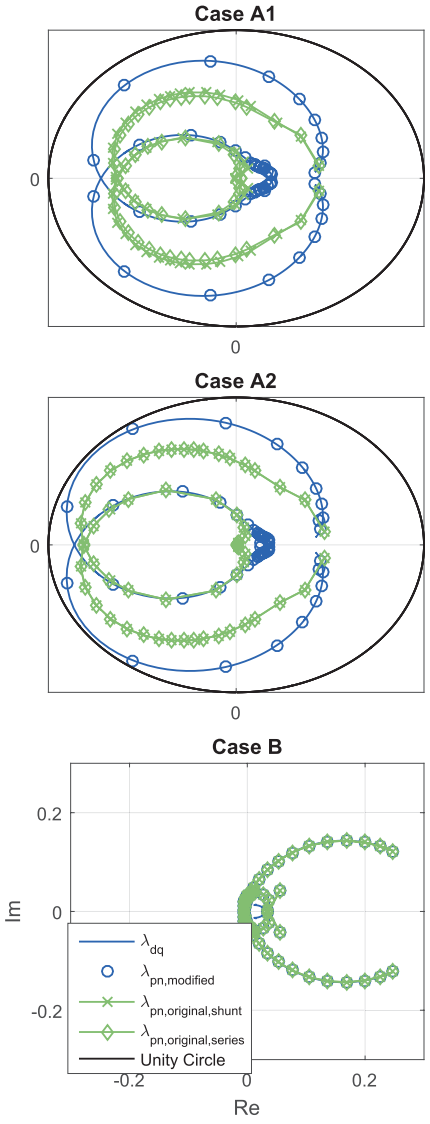

Fig. 16. Comparison of Nyquist plots for cases A1, A2, and B.

in both i_{sd} and i_{sq} are gradually increasing until instability occurs at the reference value of 1.2 p.u. Note that a reference value of 1.1 p.u. is the basis for the Nyquist plot in Fig. 16 as indicated by arrows. This operation point has poorly damped oscillations, supporting the fact that the Nyquist plot is close to encircling the point $(-1, 0)$. It can be observed that case A2 has stronger oscillations, which is also indicated by its Nyquist plot being closer to $(-1, 0)$ compared to case A1.

VI. DISCUSSION

After the derivations and proofs presented in the previous sections, it is useful to discuss the advantages and disadvantages of the two impedance domains. In this discussion, the modified sequence domain is assumed because the original definition has been shown to be ambiguous and can be inaccurate for systems that are not MFD.

The general statement is that the two domains are equivalent. The impedance matrix in one domain can be obtained from the other through a linear transformation where the eigenvalues are preserved. Hence, both domains should

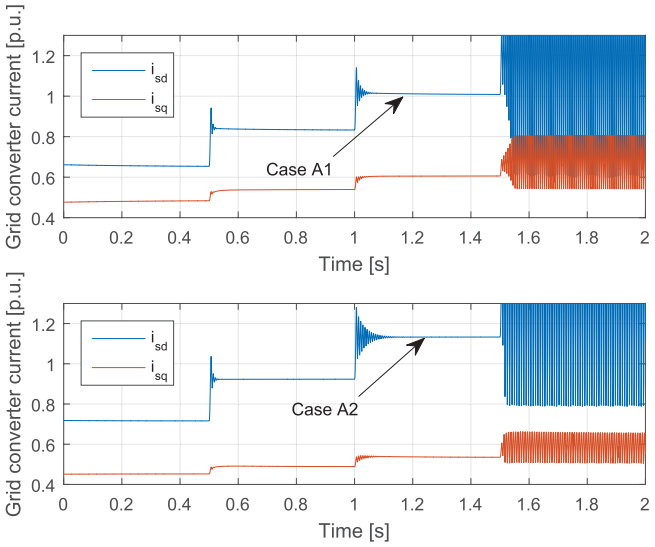

Fig. 17. Time-domain analysis of cases A1 and A2. Grid converter dq currents during stepwise increase in I_{dc}. Arrows indicate the operation point used for impedance calculations.

provide the same results. However, from a more practical viewpoint, there are a few advantages with the sequence domain over dq, especially when impedances are obtained from simulation or measurements.

1) There is no need to perform dq transformations to any measured signal, and hence no need for a reference transformation angle.
2) The off-diagonal terms in the sequence-domain impedance matrix will often have low values and are equal to zero for an MFD system. In other words, the sequence-domain impedance matrix is close to decoupled.
3) It can be argued that the sequence domain can be intuitively associated with a physical meaning and is less abstract than the dq domain.

The main advantage with the dq domain is that most previous studies on the control and stability of power electronics converters have been performed in dq coordinates. Regarding analytical impedance models, it is also possible that the derivations are less complex in the dq domain, but this has not yet been extensively investigated.

In most of the previous work on stability analysis based on the Nyquist criterion, it has been argued that off-diagonal impedance matrix elements can be neglected. Based on the impedance matrix structure for MFD systems (21), it is clear that such simplifications are correct in the sequence domain but not in the dq domain.

This paper has shown that original sequence-domain impedances depend on injection type (shunt versus series) when *both* subsystems are non-MFD. In general, the load subsystem prefers series injection, while the source subsystem prefers shunt injection. This is due to the fact that the load subsystem has higher impedance at most frequencies. When choosing injection type for a given system, the system with more mirror frequency coupling should be prioritized. It is expected that this is often the load subsystem; in this case, series injection is more accurate.

VII. Conclusion

Stability analysis of ac power electronics systems through frequency-dependent impedance equivalents is a relatively new field of research. Both *dq-domain* and *sequence-domain* analyses have been reported in previous works. However, limited effort has been dedicated to the understanding of their equivalence with respect to the stability estimates they provide. This paper attempts to contribute in this direction by reporting the following findings.

1) A modified definition for the sequence-domain impedance matrix, which extends the original sequence-domain impedance definition. The extension is related to the ability to account for induced frequency components shifted by twice the fundamental frequency.
2) The relationship between the well-established dq-domain impedance matrix and the modified sequence-domain impedance matrix. This can be viewed as a linear transformation where many essential properties are preserved.
3) The choice of impedance domain does not affect the analysis of stability using the GNC.
4) Definition of the terms mirror frequency effect and MFD systems.
5) The modified sequence-domain impedance matrix is diagonal for MFD systems. The dq-domain impedance matrix is not diagonal.
6) The dq-domain impedance matrix can be obtained from single measurements without the need for matrix inversions when both subsystems are MFD.
7) The original sequence-domain impedance is shown to be ambiguous in the general case; it depends on injection type, and the source state variables appear in the load impedance expression, and vice versa.
8) The relationship between the original and the modified sequence-domain impedance was derived under the assumption of both ideal series and ideal shunt injection.
9) The original sequence-domain impedance no longer depends on injection type when *one* of the subsystems is MFD. However, the source state variables still appear in the load impedance expression (assuming the source is MFD).

All equations were derived mathematically on a general basis and were verified by numeric simulations. Points 1–5 were examined in Section V-C, whereas points 6–9 were examined in Section V-D.

Appendix

A. Parameter Values Used in Simulations

See Tables IV–VI.

B. Proof of Equal Determinants

The following relation proves that the determinant of $\boldsymbol{Z_{dq}}$ is always equal to the determinant of $\boldsymbol{Z_{pn}}$:

$$\begin{aligned}\det(\boldsymbol{Z_{pn}}) &= \det\left(A_Z \cdot \boldsymbol{Z_{dq}} \cdot A_Z^{-1}\right)\\ &= \det(A_Z) \cdot \det(\boldsymbol{Z_{dq}}) \cdot \det\left(A_Z^{-1}\right)\\ &= -j \cdot \det(\boldsymbol{Z_{dq}}) \cdot j = \det(\boldsymbol{Z_{dq}}).\end{aligned} \tag{26}$$

TABLE IV
PARAMETER VALUES APPLIED IN CASE A1

V_{base}= 690 V	S_{base} = 1 MW	$V_{dc,base}$= 1400 V
V_{Sdc} = 1 $p.u.$	V^*_{Ldc} = 1 $p.u.$	$Z_S = 0.007 + j0.15$ $p.u.$
$C_{dc} = 11.5$ mF	$I_{dc} = 1.1$ $p.u.$	$Z_L = 0.02 + j0.25$ $p.u.$
L_{vd}= 0.0 $p.u.$	K_{pvd} = 1 $p.u.$	T_{ivd}= 0.1 s
L_{vq}= 0.2 $p.u.$	K_{pvq} = 1.3 $p.u.$	T_{ivq}= 0.2 s
K_{pid} = 1.59 $p.u.$	T_{iid}= 0.047 s	f_n= 50 Hz
K_{piq} = 2.07 $p.u.$	T_{iiq}= 0.033 s	K_{pvdc} = 8.33 $p.u.$
T_{ivdc} = 0.0036 s	$v^*_d = 1.0$ $p.u.$	$v^*_q = 0.0$ $p.u.$
$i^*_{Lq} = 0.4$ $p.u.$		

TABLE V
PARAMETER VALUES APPLIED IN CASE A2. PARAMETERS IN RED ARE DIFFERENT FROM CASE A1

V_{base}= 690 V	S_{base} = 1 MW	$V_{dc,base}$= 1400 V
V_{Sdc} = 1 $p.u.$	V^*_{Ldc} = 1 $p.u.$	$Z_S = 0.007 + j0.15$ $p.u.$
$C_{dc} = 11.5$ mF	$I_{dc} = 1.1$ $p.u.$	$Z_L = 0.02 + j0.25$ $p.u.$
L_{vd}= 0.1 $p.u.$	K_{pvd} = 1 $p.u.$	T_{ivd}= 0.1 s
L_{vq}= 0.1 $p.u.$	K_{pvq} = 1 $p.u.$	T_{ivq}= 0.1 s
K_{pid} = 1.59 $p.u.$	T_{iid}= 0.047 s	f_n= 50 Hz
K_{piq} = 2.07 $p.u.$	T_{iiq}= 0.033 s	K_{pvdc} = 8.33 $p.u.$
T_{ivdc} = 0.0036 s	$v^*_d = 1.0$ $p.u.$	$v^*_q = 0.0$ $p.u.$
$i^*_{Lq} = 0.4$ $p.u.$		

TABLE VI
PARAMETER VALUES APPLIED IN CASE B. PARAMETERS IN RED ARE DIFFERENT FROM CASE A2

V_{base}= 690 V	S_{base} = 1 MW	$V_{dc,base}$= 1400 V
V_{Sdc} = 1 $p.u.$	V_{Ldc} = 1 $p.u.$	$Z_S = 0.007 + j0.15$ $p.u.$
$C_{dc} = 11.5$ mF	$i^*_{Ld} = 1.1$ $p.u.$	$Z_L = 0.02 + j0.25$ $p.u.$
L_{vd}= 0.1 $p.u.$	K_{pvd} = 1 $p.u.$	T_{ivd}= 0.1 s
L_{vq}= 0.1 $p.u.$	K_{pvq} = 1 $p.u.$	T_{ivq}= 0.1 s
K_{pid} = 1.59 $p.u.$	T_{iid}= 0.047 s	f_n= 50 Hz
K_{piq} = 1.59 $p.u.$	T_{iiq}= 0.047 s	$i^*_{Lq} = 0.4$ $p.u.$
$v^*_d = 1.0$ $p.u.$	$v^*_q = 0.0$ $p.u.$	

C. Proof of MFD Impedance Matrices Relations (21)

When a subsystem is assumed MFD, the off-diagonal elements in $\boldsymbol{Z_{pn}}$ are equal to zero by definition. Hence, $Z_{pn} = Z_{np} = 0$. Substituting from (13) then gives

$$Z_{pn} = \frac{1}{2}[1 \quad -j]\boldsymbol{Z_{dq}}\begin{bmatrix}1\\-j\end{bmatrix} = 0$$
$$Z_{np} = \frac{1}{2}[1 \quad j]\boldsymbol{Z_{dq}}\begin{bmatrix}1\\j\end{bmatrix} = 0. \tag{27}$$

Expanding these expressions by substituting from (9) gives

$$\begin{aligned} Z_{dd} &= Z_{qq} = Z_{\text{diag}} \\ Z_{dq} &= -Z_{qd} = Z_{\text{offdiag}} \\ Z_{pp} &= \frac{Z_{\text{diag}} - jZ_{\text{offdiag}}}{2} \\ Z_{nn} &= \frac{Z_{\text{diag}} + jZ_{\text{offdiag}}}{2}. \end{aligned} \tag{28}$$

Z_{diag} and Z_{offdiag} are defined in (21).

D. Relationship Between Modified and Original Sequence-Domain Impedance Definitions

1) General Case: The relationship between the modified sequence-domain impedance definition (14) and the original (1) can be derived by solving (11) for the source and load subsystems simultaneously. When specifying the set of equations, one must choose between shunt current and series voltage injection, and between positive and negative sequence injection.

One should choose positive sequence injection in order to find the positive sequence impedance Z_p and negative sequence injection to find Z_n. The following set of equations should be solved to obtain the impedance Z_p for shunt current injection. This is equivalent to solving the circuit presented in Fig. 2

$$\begin{aligned} V_p^L &= I_p^L Z_{pp}^L + I_n^L Z_{pn}^L \\ V_n^L &= I_p^L Z_{np}^L + I_n^L Z_{nn}^L \\ V_p^S &= I_p^S Z_{pp}^S + I_n^S Z_{pn}^S \\ V_n^S &= I_p^S Z_{np}^S + I_n^S Z_{nn}^S \\ V_p^L &= V_p^S = V_p \\ V_n^L &= V_n^S = V_n \\ I_n^S &= -I_n^L \\ Z_p^L|_{\text{shunt}} &= \frac{V_p}{I_p^L} \\ Z_p^S|_{\text{shunt}} &= \frac{V_p}{I_p^S}. \end{aligned} \tag{29}$$

The superscript L denotes the load subsystem, whereas S denotes the source subsystem. The first four equations are the generalized Ohm's law with the modified sequence domain definition. The last five equations depend on the choice of injection type, as well as the choice of positive or negative sequence injection. The voltages in the two subsystems are equal if the injection is shunt type. Furthermore, the sum of negative sequence current must be zero because the injected perturbation is assumed to be a pure positive sequence. Solving (29) gives the following *original* impedance:

$$\begin{aligned} Z_p^L|_{\text{shunt}} &= \frac{V_p}{I_p^L} = \frac{Z_{pp}^L D^S + Z_{pp}^S D^L}{D^S + Z_{nn}^L Z_{pp}^S - Z_{pn}^L Z_{np}^S} \\ Z_p^S|_{\text{shunt}} &= \frac{V_p}{I_p^S} = \frac{Z_{pp}^S D^L + Z_{pp}^L D^S}{D^L + Z_{nn}^S Z_{pp}^L - Z_{pn}^S Z_{np}^L} \end{aligned} \tag{30}$$

where D^S and D^L are the determinants of the source and load impedance matrices, respectively

$$\begin{aligned} D^S &= Z_{dd}^S Z_{qq}^S - Z_{dq}^S Z_{qd}^S = Z_{pp}^S Z_{nn}^S - Z_{pn}^S Z_{np}^S \\ D^L &= Z_{dd}^L Z_{qq}^L - Z_{dq}^L Z_{qd}^L = Z_{pp}^L Z_{nn}^L - Z_{pn}^L Z_{np}^L. \end{aligned} \tag{31}$$

It is shown in Appendix B that the determinant of $\boldsymbol{Z_{pn}}$ equals the determinant of $\boldsymbol{Z_{dq}}$.

A corresponding expression can be derived for series-voltage positive sequence injection. The last five equations in (29) are then modified to

$$\begin{aligned} I_p^L &= -I_p^S = I_p \\ I_n^L &= -I_n^S = I_n \\ V_n^S &= V_n^L \\ Z_p^L|_{\text{series}} &= \frac{V_p^L}{I_p} \\ Z_p^S|_{\text{series}} &= \frac{V_p^S}{I_p}. \end{aligned} \tag{32}$$

Solving the set of equations gives

$$Z_p^L\big|_{\text{series}} = \frac{V_p^L}{I_p} = \frac{Z_{pp}^L Z_{nn}^S - Z_{pn}^L Z_{np}^S + D^L}{Z_{nn}^S + Z_{nn}^L}$$
$$Z_p^S\big|_{\text{series}} = \frac{V_p^S}{I_p} = \frac{Z_{pp}^S Z_{nn}^L - Z_{pn}^S Z_{np}^L + D^S}{Z_{nn}^L + Z_{nn}^S}. \quad (33)$$

Given that (33) clearly differs from (30), it can be concluded that the original sequence domain impedance is not well defined in the general case because it depends on the injection type. This has been illustrated by simulations in Fig. 13.

The additional equations for negative sequence are given in

$$Z_n^L\big|_{\text{shunt}} = \frac{V_n}{I_n^L} = \frac{Z_{nn}^L D^S + Z_{nn}^S D^L}{D^S + Z_{pp}^L Z_{nn}^S - Z_{np}^L Z_{pn}^S}$$
$$Z_n^L\big|_{\text{series}} = \frac{V_n^L}{I_n} = \frac{Z_{nn}^L Z_{pp}^S - Z_{np}^L Z_{pn}^S + D^L}{Z_{pp}^S + Z_{pp}^L}$$
$$Z_n^S\big|_{\text{shunt}} = \frac{V_n}{I_n^S} = \frac{Z_{nn}^S D^L + Z_{nn}^L D^S}{D^L + Z_{pp}^S Z_{nn}^L - Z_{np}^S Z_{pn}^L}$$
$$Z_n^S\big|_{\text{series}} = \frac{V_n^S}{I_n} = \frac{Z_{nn}^S Z_{pp}^L - Z_{np}^S Z_{pn}^L + D^S}{Z_{pp}^L + Z_{pp}^S}. \quad (34)$$

In Section V, these analytic expressions are validated through a comparison where the original sequence impedances are obtained directly by simulation.

2) Special Case With One MFD Subsystem: In the special case where one subsystem is MFD, the expressions from the previous sections can be simplified. If the source subsystem is MFD, i.e., $Z_{pn}^S = Z_{np}^S = 0$, then, (30), (33), and (34) are reduced to

$$Z_p^L\big|_{\text{shunt}} = Z_p^L\big|_{\text{series}} = Z_{pp}^L - \frac{Z_{pn}^L Z_{np}^L}{Z_{nn}^S + Z_{nn}^L}$$
$$Z_p^S\big|_{\text{shunt}} = Z_p^S\big|_{\text{series}} = Z_{pp}^S$$
$$Z_n^L\big|_{\text{shunt}} = Z_n^L\big|_{\text{series}} = Z_{nn}^L - \frac{Z_{np}^L Z_{pn}^L}{Z_{pp}^S + Z_{pp}^L}$$
$$Z_n^S\big|_{\text{shunt}} = Z_n^S\big|_{\text{series}} = Z_{nn}^S. \quad (35)$$

Three important observations are obtained from (35). As expected, in the source subsystem, the original and modified impedances are equal, i.e., $Z_p^S = Z_{pp}^S$ because this subsystem is MFD. Second, in the load subsystem, the original sequence-domain impedance no longer depends on injection type, i.e., $Z_p^L|_{\text{shunt}} = Z_p^L|_{\text{series}}$. The third observation is that $Z_p^L \neq Z_{pp}^L$. The difference between them is proportional to $Z_{pn}^L Z_{np}^L$, and also depends on the source impedance Z_{nn}^S. These observations can be seen in the simulation result shown in Fig. 14.

E. Special Case in Which Both Subsystems Are MFD

In this case, (30), (33), and (34) are reduced to

$$Z_p^L\big|_{\text{shunt}} = Z_p^L\big|_{\text{series}} = Z_{pp}^L$$
$$Z_p^S\big|_{\text{shunt}} = Z_p^S\big|_{\text{series}} = Z_{pp}^S$$
$$Z_n^L\big|_{\text{shunt}} = Z_n^L\big|_{\text{series}} = Z_{nn}^L$$
$$Z_n^S\big|_{\text{shunt}} = Z_n^S\big|_{\text{series}} = Z_{nn}^S. \quad (36)$$

In other words, the original and modified sequence-domain impedances are equal. This was also shown by (21) and demonstrates the fact that MFD is a sufficient assumption for the original sequence-domain impedances to be uniquely defined. The corresponding simulation result is shown in Fig. 15.

REFERENCES

[1] J. Sun, "Small-signal methods for AC distributed power systems—A review," *IEEE Trans. Power Electron.*, vol. 24, no. 11, pp. 2545–2554, Nov. 2009.

[2] M. Belkhayat, *Stability Criteria for AC Power Systems With Regulated Loads*. West Lafayette, IN, USA: Purdue Univ., 1997.

[3] R. D. Middlebrook, "Input filter considerations in design and application of switching regulators," in *Proc. IEEE Ind. Appl. Soc. Annu. Meeting*, Oct. 1976.

[4] G. Francis, R. Burgos, D. Boroyevich, F. Wang, and K. Karimi, "An algorithm and implementation system for measuring impedance in the D-Q domain," in *Proc. IEEE Energy Convers. Congr. Expo. (ECCE)*, Sep. 2011, pp. 3221–3228.

[5] Y. A. Familiant, J. Huang, K. A. Corzine, and M. Belkhayat, "New techniques for measuring impedance characteristics of three-phase AC power systems," *IEEE Trans. Power Electron.*, vol. 24, no. 7, pp. 1802–1810, Jul. 2009.

[6] J. Huang, K. A. Corzine, and M. Belkhayat, "Small-signal impedance measurement of power-electronics-based AC power systems using line-to-line current injection," *IEEE Trans. Power Electron.*, vol. 24, no. 2, pp. 445–455, Feb. 2009.

[7] T. Roinila, M. Vilkko, and J. Sun, "Online grid impedance measurement using discrete-interval binary sequence injection," *IEEE J. Emerg. Sel. Topics Power Electron.*, vol. 2, no. 4, pp. 985–993, Dec. 2014.

[8] M. Cespedes and J. Sun, "Adaptive control of grid-connected inverters based on online grid impedance measurements," *IEEE Trans. Sustain. Energy*, vol. 5, no. 2, pp. 516–523, Apr. 2014.

[9] N. Hoffmann and F. W. Fuchs, "Minimal invasive equivalent grid impedance estimation in inductive–resistive power networks using extended Kalman filter," *IEEE Trans. Power Electron.*, vol. 29, no. 2, pp. 631–641, Feb. 2014.

[10] P. Xiao, G. K. Venayagamoorthy, K. A. Corzine, and J. Huang, "Recurrent neural networks based impedance measurement technique for power electronic systems," *IEEE Trans. Power Electron.*, vol. 25, no. 2, pp. 382–390, Feb. 2010.

[11] B. Wen, D. Dong, D. Boroyevich, R. Burgos, P. Mattavelli, and Z. Shen, "Impedance-based analysis of grid-synchronization stability for three-phase paralleled converters," *IEEE Trans. Power Electron.*, vol. 31, no. 1, pp. 26–38, Jan. 2015.

[12] M. Cespedes and J. Sun, "Impedance modeling and analysis of grid-connected voltage-source converters," *IEEE Trans. Power Electron.*, vol. 29, no. 3, pp. 1254–1261, Mar. 2014.

[13] X. Wang, F. Blaabjerg, and W. Wu, "Modeling and analysis of harmonic stability in an AC power-electronics-based power system," *IEEE Trans. Power Electron.*, vol. 29, no. 12, pp. 6421–6432, Dec. 2014.

[14] R. Turner, S. Walton, and R. Duke, "A case study on the application of the Nyquist stability criterion as applied to interconnected loads and sources on grids," *IEEE Trans. Ind. Electron.*, vol. 60, no. 7, pp. 2740–2749, Jul. 2013.

[15] C. A. Desoer and Y.-T. Wang, "On the generalized Nyquist stability criterion," *IEEE Trans. Autom. Control*, vol. 25, no. 2, pp. 187–196, Apr. 1980.

[16] Z. Liu, J. Liu, W. Bao, and Y. Zhao, "Infinity-norm of impedance-based stability criterion for three-phase AC distributed power systems with constant power loads," *IEEE Trans. Power Electron.*, vol. 30, no. 6, pp. 3030–3043, Jun. 2015.

[17] C. M. Wildrick, F. C. Lee, B. H. Cho, and B. Choi, "A method of defining the load impedance specification for a stable distributed power system," *IEEE Trans. Power Electron.*, vol. 10, no. 3, pp. 280–285, May 1995.

[18] J. Sun, "Impedance-based stability criterion for grid-connected inverters," *IEEE Trans. Power Electron.*, vol. 26, no. 11, pp. 3075–3078, Nov. 2011.

[19] R. Burgos, D. Boroyevich, F. Wang, K. Karimi, and G. Francis, "On the AC stability of high power factor three-phase rectifiers," in *Proc. IEEE Energy Convers. Congr. Expo. (ECCE)*, Sep. 2010, pp. 2047–2054.

[20] D. Dong, B. Wen, D. Boroyevich, P. Mattavelli, and Y. Xue, "Analysis of phase-locked loop low-frequency stability in three-phase grid-connected power converters considering impedance interactions," *IEEE Trans. Ind. Electron.*, vol. 62, no. 1, pp. 310–321, Jan. 2015.
[21] B. Wen, D. Boroyevich, R. Burgos, P. Mattavelli, and Z. Shen, "Small-signal stability analysis of three-phase AC systems in the presence of constant power loads based on measured $d-q$ frame impedances," *IEEE Trans. Power Electron.*, vol. 30, no. 10, pp. 5952–5963, Oct. 2015.
[22] B. Wen, D. Boroyevich, R. Burgos, P. Mattavelli, and Z. Shen, "Analysis of D-Q small-signal impedance of grid-tied inverters," *IEEE Trans. Power Electron.*, vol. 31, no. 1, pp. 675–687, Jan. 2016.
[23] Z. Bing, "Three-phase AC-DC converters for more-electric aircraft," Ph.D. dissertation, Dept. Elect. Eng., Rensselaer Polytech. Inst., Troy, NY, USA, 2010.
[24] V. Valdivia, A. Lazaro, A. Barrado, P. Zumel, C. Fernandez, and M. Sanz, "Black-box modeling of three-phase voltage source inverters for system-level analysis," *IEEE Trans. Ind. Electron.*, vol. 59, no. 9, pp. 3648–3662, Sep. 2012.
[25] M. Cespedes and J. Sun, "Three-phase impedance measurement for system stability analysis," in *Proc. IEEE 14th Workshop Control Modeling Power Electron. (COMPEL)*, Jun. 2013, pp. 1–6.
[26] M. K. Bakhshizadeh *et al.*, "Couplings in phase domain impedance modeling of grid-connected converters," *IEEE Trans. Power Electron.*, vol. 31, no. 10, pp. 6792–6796, Oct. 2016.
[27] D. N. Zmood, D. G. Holmes, and G. H. Bode, "Frequency-domain analysis of three-phase linear current regulators," *IEEE Trans. Ind. Appl.*, vol. 37, no. 2, pp. 601–610, Mar./Apr. 2001.

Atle Rygg received the M.Sc. degree in electrical engineering from the Norwegian University of Science and Technology, Trondheim, Norway, in 2011, where he is currently pursuing the Ph.D. degree with the Department of Engineering Cybernetics.

He was a Research Scientist with SINTEF Energy Research, Trondheim, from 2011 to 2015, where he was involved in power electronics. His current research interests include impedance-based stability analysis of power electronic systems, where the aim is to contribute to the fundamental understanding in this family of methods.

Marta Molinas (M'94) received the Diploma degree in electromechanical engineering from the National University of Asunción, San Lorenzo, Paraguay, in 1992, the M.E. degree from the University of the Ryukyus, Nishihara, Japan, in 1997, and the D.Eng. degree from the Tokyo Institute of Technology, Tokyo, Japan, in 2000.

She was a Guest Researcher with the University of Padova, Padua, Italy, in 1998. From 2004 to 2007, she was a Post-Doctoral Researcher with the Norwegian University of Science and Technology (NTNU), Trondheim, Norway, where she was a Professor with the Department of Electric Power Engineering from 2008 to 2014. She is currently a Professor with the Department of Engineering Cybernetics, NTNU. Her current research interests include stability of power electronics systems, harmonics, instantaneous frequency, and non-stationary signals from the human and the machine.

Dr. Molinas is an Associate Editor of the IEEE JOURNAL OF EMERGING AND SELECTED TOPICS IN POWER ELECTRONICS and the IEEE TRANSACTIONS ON POWER ELECTRONICS and an Editor of the IEEE TRANSACTIONS ON ENERGY CONVERSION. She was an AdCom Member of the IEEE Power Electronics Society from 2009 to 2011.

Chen Zhang received the B.Eng. degree in electrical engineering from the China University of Mining and Technology, Xuzhou, China, in 2011. He is currently pursuing the Ph.D. degree in electrical engineering with Shanghai Jiao Tong University, Shanghai, China.

He was a Ph.D. Visiting Scholar with the Department of Engineering Cybernetics, Norwegian University of Science and Technology, Trondheim, Norway, in 2015. His current research interests include dynamic modeling of VSC-based energy conversion systems and stability analysis of power electronic energized power system.

Xu Cai received the B.Eng. degree from Southeast University, Nanjing, China, in 1983, and the M.Sc. and Ph.D. degrees from the China University of Mining and Technology, Xuzhou, China, in 1988 and 2000, respectively.

He was with the Department of Electrical Engineering, China University of Mining and Technology, as an Associate Professor from 1989 to 2001. He was the Vice Director of the State Energy Smart Grid R&D Center, Shanghai, China, from 2010 to 2013. He has been with Shanghai Jiao Tong University, Shanghai, as a Professor since 2002, where he has also been the Director of the Wind Power Research Center since 2008. His current research interests include power electronics and renewable energy exploitation and utilization, including wind power converters, wind turbine control system, large power battery storage systems, clustering of wind farms and its control system, and grid integration.